**Proceedings of the ASME 2018 37th International
Conference on Ocean, Offshore and Arctic Engineering
OMAE2018
June 17-22, 2018, Madrid, Spain**

OMAE2018-77776

MODELLING AND SIMULATION OF MOORED-FLOATING STRUCTURES USING THE TENSION-ELEMENT-METHOD

Tobias Martin[*]
Marine Civil Engineering
Department of Civil and Environmental Engineering
Norwegian University of Science and Technology (NTNU)
Trondheim, Norway
Email: tobias.martin@ntnu.no

Arun Kamath
Hans Bihs
Marine Civil Engineering
Department of Civil and Environmental Engineering
Norwegian University of Science and Technology (NTNU)
Trondheim, Norway

ABSTRACT

The application of a discrete mooring model for floating structures is presented in this paper. The method predicts the steady-state solution for the shape of an elastic cable and the tension forces under consideration of static loads. It is based on a discretization of the cable in mass points connected with straight but elastic bars. The successive approximation is applied to the resulting system of equations which leads to a significant reduction of the matrix size in comparison to the matrix of a Newton-Raphson method. The mooring model is implemented in the open-source CFD model REEF3D. The solver has been used to study various problems in the field of wave hydrodynamics and fluid-structure interaction. It includes floating structures through a level set function and captures its motion using Newton and Euler equations in 6DOF. The fluid-structure interaction is solved explicitly using an immersed boundary method based on the ghost cell method. The applications show the accuracy of the solver and effects of mooring on the motion of floating structures.

INTRODUCTION

Mooring systems ensure the safety of structures near the shore such as floating breakwaters and aquaculture cages by keeping them in position. Their design has either to provide enough flexibility to allow large displacements or enough strength to withstand the hydrodynamic loads while restraining the structural motion. The accurate determination of the motion of the moored structure and the resulting tension forces in the cables are, therefore, of high significance to produce a safe and economical design. If the motion of the floating structure is large, mooring dynamics can have a significant impact on the response of the structure. The general solution for the dynamics of mooring systems has to be found numerically due to the underlying non-linear system of equations. A general overview of different solution methods can be found in [1]. One group of methods is based on splitting the cable in finite differences or finite elements, as can be found in [2] and [3]. Alternatively, the lumped mass method [4] was developed which applies truss or spring elements for the discretization. A system of equations is generated from force equilibria at each mass knot, and the solution is found for the knot positions. Even though these methods show accurate results for dynamic and static problems, they lack a mechanism to prevent unphysical correlation of tension forces and twine deformations. At this point, the tension element method (TEM) [5, 6] presents a suitable alternative because it incorporates this correlation by including a geometrical constraint. It is formulated using the necessary connection between the elements at any time. The method is also based on a discretization in a finite number of mass points which are connected by straight but elastic bars. However, it is limited to quasi-static cases which is suitable if

---

[*]Address all correspondence to this author.

Copyright © 2018 ASME

the exact motion of the cable is not of interest. The neglection of time-dependency provides the possibility to find the unit vectors of the bars as the solution of the system. This simplifies the interpretation of both the theoretical approach and the evaluation of the physical results because the length of the bars, tension forces in the bars and the displacement of the knots are direct solutions of the calculations [7]. Further, the system can be solved by applying successive approximation. Here, the unknowns are separated, and the system is corrected iteratively using the intermediate results until convergence has been reached. [5] shows the conversion of the system for using a Newton-Raphson method which is though more expensive in runtime. It is caused by an increase of the matrix size because all unknowns have to be written into the solution vector instead of splitting them.

The mooring model is implemented in the open-source CFD code REEF3D [8]. The model has been used and validated for a wide range of marine applications, such as breaking wave kinematics [9], breaking wave forces [10] and sloshing [11]. For floating bodies, an extension of the local directional immersed boundary method [12] using the field extension method [13] is implemented. The geometry of the solid is described by a level-set function. Hence, forces and moments can be calculated without explicitly defining the intersections between the surface mesh and the grid of the flow domain. Like other immersed boundary methods (see e.g, [14, 15]), the solid body is immersed into the fluid and re-meshing or overset grids [16] are avoided. A weak coupling between fluid and structure is applied which results in a stable model with accurate results for various applications [17, 18].

In the following, details about the numerical models for the fluid-structure interaction and for the mooring system are presented. Afterwards, the solver is applied to a moored-floating barge and the heave motion of a sphere.

NUMERICAL MODEL

The basic equations which are solved in the whole domain are represented by the continuity equation and conservation of momentum for incompressible fluids, which are given as

$$\frac{\partial u_i}{\partial x_i} = 0,$$

$$\frac{\partial u_i}{\partial t} + u_j \frac{\partial u_i}{\partial x_j} = -\frac{1}{\rho} \frac{\partial p}{\partial x_i} + \frac{\partial}{\partial x_j} \left(\nu \cdot \left(\frac{\partial u_i}{\partial x_j} + \frac{\partial u_j}{\partial x_i} \right) \right) + g_i, \quad (1)$$

with u_i the velocity components, ρ the fluid density, p the pressure, ν the kinematic viscosity and $\vec{g}$ the gravity acceleration vector. The Reynolds-averaged Navier-Stokes (RANS) equations are solved by replacing the fluid properties with time-averaged values and add turbulent viscosity to ν. The additional viscosity is calculated with a modified k-ω model as given in [8].

A finite difference method (FDM) on a Cartesian grid is used for the discretization of the spatial domain. System (1) is solved on a staggered grid to avoid decoupling of pressure and velocity. Convection terms are evaluated in a non-conservative form because the violation of the mass conservation during an explicit solution procedure might cause numerical instabilities in a conservative formulation [19]. For this purpose, the fifth-order accurate weighted essentially non-oscillatory (WENO) scheme [20] adapted to non-conservative terms [21] is applied. The discretised system is solved using Chorin's projection method for incompressible flows [22]. The pressure is calculated from a Poisson equation and solved using a fully parallelized BiCGStab algorithm [23]. For the progress in time, the third-order accurate Total Variation Diminishing (TVD) RungeKutta scheme [24] is employed. Adaptive time stepping controls the time stepping according to the required CFL condition. The location of the free water surface is represented implicitly by the zero level set of a smooth signed distance function which is defined as the closest distance to the interface [25]. Its motion can be described by the advection equation. The convection term is discretised by the fifth-order accurate Hamilton-Jacobi WENO method of [26]. In order to conserve the signed distance property, the level set function is reinitialized after each time step. Here, the PDE-based reinitialization equation of [19] is taken into account. The material properties of the two phases are finally determined for the whole domain in accordance with the continuum surface force model of [27].

6DOF ALGORITHM

The rigid body is defined by the location of its centre of gravity and its orientation in the inertial coordinate system, which is described by Euler angles in this paper. The resulting position vector $\vec{x} = (x_1, ..., x_6)^T$ consists of the translational components, describing the coordinates of the centre of gravity, and the three Euler angles ϕ, θ and ψ. The calculation of the motion of a body in the inertial system would include several time derivatives of moments which can be avoided by applying a coordinate transformation. For this purpose, the rotation components in the principal coordinate system of the body are represented by $\vec{\xi} = (\xi_1, \xi_2, \xi_3)^T$. In the principal axes system of the body, the inertia tensor reduces to the three principal moments of inertia $\vec{I} = diag(I_j) = diag(mr_j^2)$, $j = x, y, z$, with m the mass of the body and r_x, r_y, r_z the distances of a point from the centre of gravity along the x-, y- and z-direction. The acting moments in this system $\vec{M}_{\vec{x}}$ have to be transformed to the non-inertial system by applying

$$\vec{M}_{\vec{\xi}} = \left(M_{1,\vec{\xi}}, M_{2,\vec{\xi}}, M_{3,\vec{\xi}} \right)^T = \vec{J}_1^{-1} \cdot \vec{M}_{\vec{x}}, \quad (2)$$

2

Copyright © 2018 ASME

with $\vec{M}_{\vec{\xi}}$ the moments in the system of the body and $\vec{J}_1^{-1}$ the rotation matrix of [28]. The translational motion of the rigid body is described by

$$\begin{pmatrix} \ddot{x}_1 \\ \ddot{x}_2 \\ \ddot{x}_3 \end{pmatrix} = \frac{1}{m} \cdot \begin{pmatrix} F_{x_1,\vec{x}} \\ F_{x_2,\vec{x}} \\ F_{x_3,\vec{x}} \end{pmatrix}, \qquad (3)$$

where $F_{\vec{x}}$ are the acting forces in the inertial system. The position of the body can be calculated analytically by integrating (3) twice. The rotatory motions are calculated from the Euler equations in the non-inertial system [28]

$$\begin{aligned} I_x \ddot{\xi}_1 + \dot{\xi}_2 \dot{\xi}_3 \cdot (I_z - I_y) &= M_{1,\vec{\xi}}, \\ I_y \ddot{\xi}_2 + \dot{\xi}_1 \dot{\xi}_3 \cdot (I_x - I_z) &= M_{2,\vec{\xi}}, \\ I_z \ddot{\xi}_3 + \dot{\xi}_1 \dot{\xi}_2 \cdot (I_y - I_x) &= M_{3,\vec{\xi}}, \qquad (4) \end{aligned}$$

which is solved explicitly using the second-order accurate Adams-Bashforth scheme. The Euler angles in the body system cannot be calculated from the body angular velocities due to missing physical interpretation. Instead, the angular velocities are transformed back using another rotation matrix (see [28] for details). Afterwards, the necessary Euler angles are calculated in the inertial frame.

In the presented calculations, the fluid-structure coupling is arranged in a weak form without sub-iterations. Hence, acting forces are calculated from the fluid using a level set function representing the body first. Afterwards, the body position is determined from (3) and (4). Finally, the fluid properties are updated to the new time level using the ghost cell immersed boundary method [12] for incorporating the boundary conditions of the solid. For both, the velocities and the pressure, these conditions are calculated from the motion of the body with respect to its centre of gravity [17]. This method shows good numerical stability throughout the range of application. However, pressure oscillations can occur in the vicinity of the solid body because of solid cells turning into fluid cells. The fresh fluid cells lack physical information about velocities from previous time steps. It is solved by implementing the field extension method of [13, 29] adapted to the ghost cell immersed boundary method.

MOORING MODEL

Each cable has a length l with the diameter d and is fixed at two points $P^{(0)}$ and $P^{(N)}$. Its discretization is represented by $N-1$ massless bars with length a and N mass points (knots) P, where all acting forces are concentrated. These are the gravity force $\vec{F}_G$ and a hydrodynamic force $\vec{F}_H$ arising from the relative motion between the structure and surrounding fluid, which is however
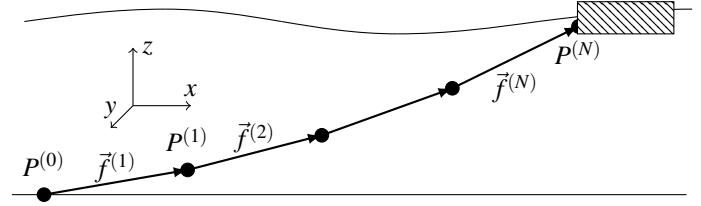

FIGURE 1: DISCRETE CABLE: MASS POINTS (BLACK POINTS), BARS (VECTORS).

neglected here. Further, no moments occur at the knots since a flexible system is assumed. The inner tension forces with magnitude F_T act at P in the direction of the adjacent bars, denoted by the unit vectors $\vec{f}$. The elasticity of the material is respected by representing a as a functional of tension forces. In this paper, the linear dependency of Hook's law is taken into account. An exemplary discretization is shown in figure 1.

The mass of the bars are distributed uniformly on the bordered knots which results in an approximated gravity force $\vec{F}_G^{(v)}$ at any knot P^v

$$\vec{F}_G^{(v)} = q\vec{g} \cdot \left(\frac{a^{(v)} + a^{(v+1)}}{2} \right), \quad v = 1, ..., N-1, \qquad (5)$$

with q the specific material weight per length in the fluid and $\vec{g}$ an unit vector pointing in negative $z-$direction.

Following the tension element method (TEM) in [5], a solution for the steady-state shape of the cable and the distribution of tension forces in the bars can be found. Both properties relate to the unknown direction of the bar unit vectors. Since the cable is fixed, the sought properties are the directions of inner bar unit vectors $\vec{f}^{(v)}$, the magnitude of the tension forces in these directions $F_T^{(v)}$ and the length of the bars $a^{(v)}$. Hence, an iterative method has to be considered for solving this problem. The system of equations is filled using force equilibria for knots and a geometrical constraint. Assuming time independence and negligence of interactions between different bars and knots, a static equation of force equilibrium yields for each inner knot of the net $P^{(v)}$

$$\vec{f}^{(v+1)} F_T^{(v+1)} - \vec{f}^{(v)} F_T^{(v)} = -\vec{F}_G^{(v)}. \qquad (6)$$

The number of bars exceeds the number of inner knots. Thus, the system is undetermined and has to be closed by adding a geometrical constraint. It accomplishes the coherence of the cable during the deformation in a physical way and is determined from the known distance between the two end points (see also figure

3

Copyright © 2018 ASME

2)

$$\sum_{v=1}^{N+1} \vec{f}^{(v)} a^{(v)} = \vec{c}. \tag{7}$$

The resulting linear system of equations can be written in an appropriate way for obtaining the matrix of unit bar vectors $\mathbf{F}$ using (6) and (7) as

$$\mathbf{A} \cdot \mathbf{F} = \mathbf{B}, \tag{8}$$

with $\mathbf{A}$ containing the sub-matrices of unknown tension forces $\mathbf{T}$ and the lengths of the bars $\mathbf{L}$

$$\mathbf{A} = \begin{pmatrix} \mathbf{T} \\ \mathbf{L} \end{pmatrix}. \tag{9}$$

On the right hand side, $\mathbf{B}$ yields

$$\mathbf{B} = \begin{pmatrix} -\mathbf{G} \\ \vec{c} \end{pmatrix}, \tag{10}$$

with $\mathbf{G}$ the sub-matrix of static forces. $\mathbf{A}$ is a square matrix with the size of the unknown bar unit vectors $N-1$, whereas $\mathbf{F}$ and $\mathbf{B}$ are matrices of size $3 \times N - 1$. Hence, the system matrix reduces significantly due to the transition from the Newton-Raphson method to the successive approximation. It yields a significant reduction of runtime under consideration of multiple inversions.

In system (8), both $\mathbf{A}$ and $\mathbf{B}$ depend on the solution matrix $\mathbf{F}$. Therefore, appropriate initial values have to be chosen for the tension forces and bar unit vectors. The solution of (8) at any iterative step (k) results then as

$$\mathbf{F}^{(k)} = \left(\mathbf{A}^{(k-1)} \right)^{-1} \cdot \mathbf{B}^{(k-1)}. \tag{11}$$

However, the lengths of bar vectors have to equal one by definition at the end of each step which cannot be guaranteed by (11) for which reason a correction step according to

$$\left(\vec{f}^{(v)} \right)^{(k*)} = \frac{\left(\vec{f}^{(v)} \right)^{(k)}}{\left| \left(\vec{f}^{(v)} \right)^{(k)} \right|}, \quad v = 1, ..., N-1, \tag{12}$$

has to be performed before the loop proceeds. In order to conserve consistency, the columns of $\mathbf{A}$ have to be multiplied by the Euclidean norm of the corresponding line of $\mathbf{F}^{(k)}$. As a matter of course, geometrical constraints are excluded from this correction. The next step $(k+1)$ can then be calculated by correcting the bar lengths in $\mathbf{A}$ and determining $\mathbf{B}$ afterwards. The algorithm stops in case of reaching a predefined criterion for the residuals of the norm like

$$|L_\infty(\mathbf{F}^{(k)}) - 1| < \kappa, \tag{13}$$

which corresponds to the conservation of all bar unit vectors within the tolerance κ.
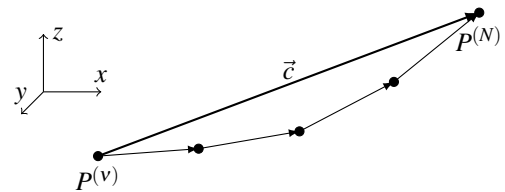

FIGURE 2: GEOMETRICAL CONSTRAINT.

RESULTS
Validation of the Tension Element Method

First, the TEM is validated using a catenary solution [30]. In general, this analytical solution provides a good approximation of the physical shape of a rope between two fixed points. As can be seen in figure 3, the numerical model converges to the catenary solution as the number of elements N increases. This is emphasised by calculating the L_2-norm of the error in z-direction, which decreases from 0.01 for $N = 3$ to 0.005 for $N = 50$.

3DOF Simulation of a Barge in Waves

Next, the 6DOF algorithm of REEF3D is analysed for the motion of a free floating barge in waves. The results are compared to the experimental data of [31]. The considered wave tank is $20m$ long, $0.8m$ high and $0.44m$ wide. The water depth in the tank is $d = 0.4m$. A rectangular barge of $0.30m \times 0.2m$ is placed inside the tank at $(x,z) = (7.0m, 0.4m)$. Its density is $500 kg/m^3$. The case can be considered as 2D because the gap between body and walls is small. Hence, the coupled motion of surge, heave and pitch motion can be investigated. The incoming waves are regular and have a height of $0.04m$, a period $T = 1.2s$ and a wavelength of $1.936m$. They are modelled using second-order Stokes wave theory. An additional numerical beach is applied in order to avoid wave reflections at the outlet. The convergence of
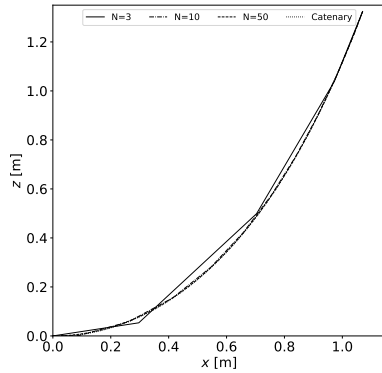
4

Copyright © 2018 ASME

FIGURE 3: NUMERICAL SOLUTION OF THE TEM USING *N* ELEMENTS IN COMPARISON TO A CATENARY SOLUTION.
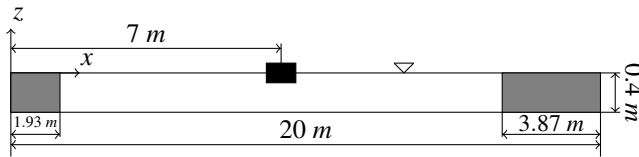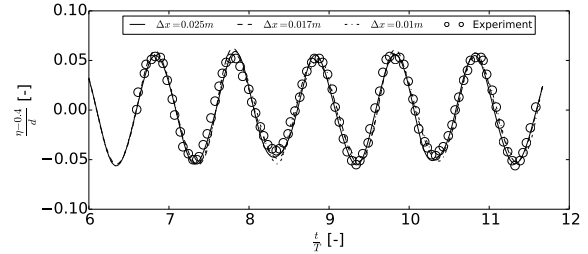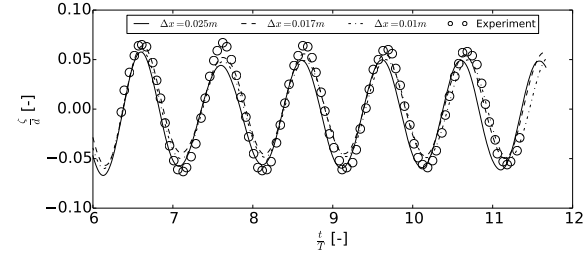

FIGURE 4: SETUP FOR THE 2D BARGE IN A NUMERICAL WAVE TANK.

the code is shown using three configurations with different cell sizes. They vary from $0.025m$ to $0.01m$, which corresponds to $25,600$ and $160,000$ cells.
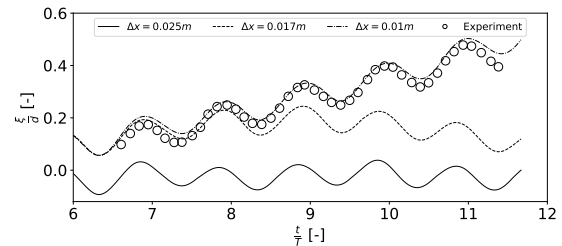
The results of the free-floating simulation are compared with the experiment for the period between $t/T = 6.36$ and $t/T = 12$. The wave elevation shown in figure 5a shows a good agreement with the experimental data, irrespective of the grid resolution. It confirms the chosen wave theory for modelling the waves and the capabilities of the solver to transport them accurately. Likewise, the predicted heave motion in figure 5b coincides with the experiments in frequency and amplitude if the grid resolution is good enough. For the finest mesh, the amplitude is however still $\approx 10\%$ too small which might be improved by further refinements. Similarly, the surge motion converges to the experiment as can be seen in figure 5c. For $\Delta x = 0.01m$, the calculated drift shows a good accordance with the experiments. The pitch motion also needs a certain grid resolution in order to be similar to the experimental data. The numerical distribution converges in frequency whereas the amplitude is still oscillating around the physical solution. The reason could be under-resolved turbulence in the vicinity of the barge which reduces the viscous damping non-physically. A further mesh refinement should, therefore, improve the results of the pitch motion.
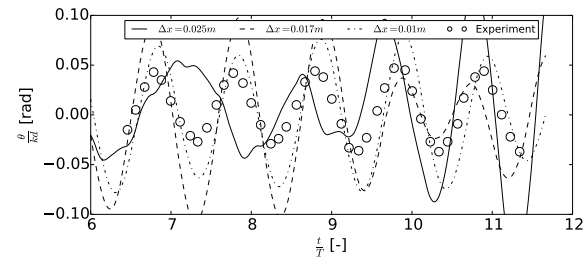

(a) WAVE ELEVATION AT $X = 5.5\ m$.

(b) HEAVE MOTION.

(c) SURGE MOTION.

(d) PITCH MOTION.

FIGURE 5: NUMERICAL RESULTS OF THE 2D BARGE IN COMPARISON TO THE EXPERIMENTAL DATA.

3DOF Simulation of a Moored Barge in Waves

The effect of mooring on the motion of the floating barge from before is shown. For this purpose, two mooring lines are fixed to the body at $z = 0.4m$. The cables are $1.9m$ long and $0.004m$ thick. Two configurations with different material weight of $q = 0.25kg/m$ and $q = 1.0kg/m$ are considered. The wave tank and barge dimensions are taken from the case above (see figure 4).

5   Copyright © 2018 ASME

However, the strong drift is prevented by decreasing the wave height and length, which are $0.02m$ and $1.336m$ here. A new simulation with a free barge and a discretization of $\Delta x = 0.01m$ is used as a reference. As the results, the heave, surge and pitch motions are shown in figure 7 between $t = 8s$ and $t = 14s$.

The lighter mooring system shows minor influences on the heave motion of the free floating barge. The draft of the body increases due to the additional weight of the system, which is obviously even more noticeable for the heavier mooring lines. Despite this, the amplitude and frequency of the motion is similar. It might be caused by the flat angle between line and body at the attachment point, resulting in a small vertical reaction force. At the same time, the surge motion in figure 7b is prevented by both mooring configurations due to the large horizontal components of the tension forces. The amplitude of the motion decreases with the increasing weight of the lines. For both configurations, the barge oscillates around the initial position with the same frequency as the heave motion. Similarly, the pitch motion is reduced by the counteracting tension forces of the two lines. As it can be seen in figure 6, a significant amount of the wave energy is extracted by the moored-floating barge, resulting more shallow and slower waves behind the body.
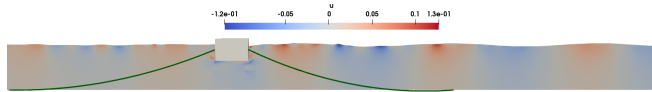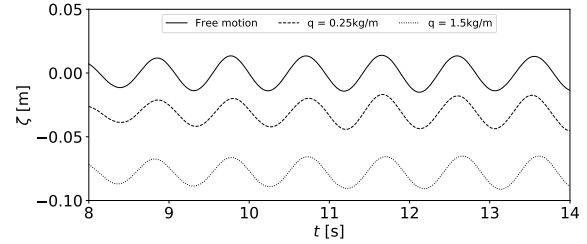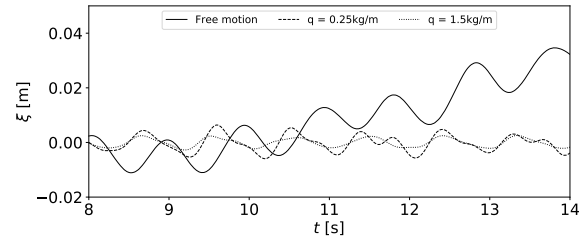

FIGURE 6: MOORED-FLOATING BARGE IN A WAVE TROUGH SITUATION (WAVES INCIDENT FROM THE RIGHT).

(a) HEAVE MOTION.

(b) SURGE MOTION.

(c) PITCH MOTION.

FIGURE 7: NUMERICAL RESULTS OF THE TWO-DIMENSIONAL BARGE WITH DIFFERENT MOORING LINES.

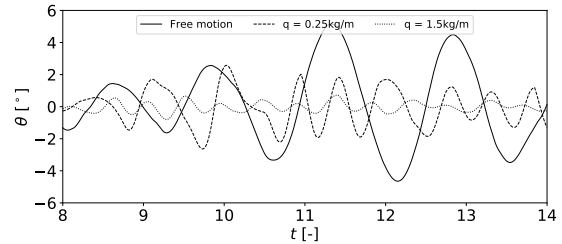## Simulating the Heave Motion of a Moored Sphere

This case is represented by a sphere with diameter $1m$ and density $500kg/m^3$ and an infinite water basin. It is numerically modelled by a rectangular domain of $10m \times 10m$ and wave absorption zones at all boundaries to prevent reflections of the waves. The sphere is moved $0.5m$ in negative z-direction as the initial condition (see also figure 8), which results in an upwards acceleration and, hence, heave motion if simulated in time. In addition, a mooring system consisting of four mooring lines is fixed at the lowest point of the sphere. Different configurations are simulated by changing the length of the mooring lines. The first configuration with $l = 3.28m$ results in slack mooring lines in the final position of the sphere (see figure 9a). In the second case, the lines are shortened to $l = 3.16m$ which corresponds to tightened lines for a large time. Finally, the mooring lines are defined to be tight in the initial condition resulting in a static equilibrium of buoyancy and tension forces after a large time as can be seen in

figure 9a. All lines are $0.004m$ thick and have a weight per unit length of $q = 0.03kg/m$ in water.

The resulting heave motion is shown in figure 10. For the free motion, the typical damped oscillation around the equilibrium at $\zeta = 0m$ of a rigid body can be observed. Introducing the mooring lines with $l = 3.28m$ and $l = 3.16m$, an increased frequency during the first periods is predicted. At the same time, the tension forces reduce the upper amplitudes of the motion but slightly increase the lower ones. This is caused by the increased acceleration of the sphere after exceeding a local maximum. Both frequency and amplitude influences, vanish in time due to the decreasing tension forces for smaller heave amplitudes. In the final configuration, a static equilibrium of forces is found at $z = -0.37m$. This location depends, in particular, on the chosen elasticity of the rope material and the weight of the sphere.
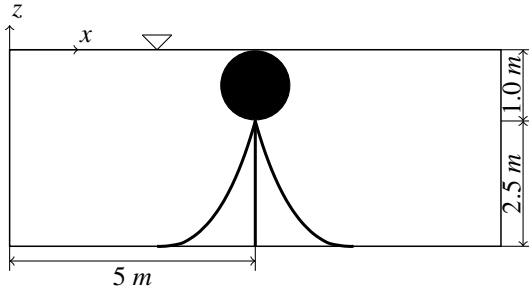
6

Copyright © 2018 ASME

FIGURE 8: SETUP FOR THE HEAVE MOTION OF A SPHERE

(a) $l = 3.28m$.

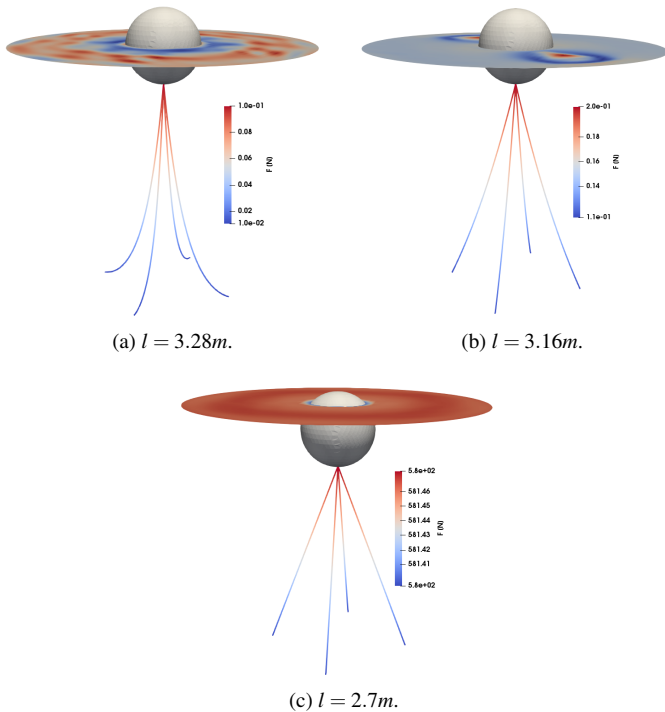(b) $l = 3.16m$.

(c) $l = 2.7m$.

FIGURE 9: SPHERE WITH DIFFERENT MOORING SYSTEMS AT $t = 14s$.

CONCLUSION

The open-source CFD model REEF3D is used in this study to evaluate the influence of different mooring systems on the motion of floating bodies. For this purpose, the tension element method is implemented which provides a fast and stable solution for quasi-stationary problems. The applications show that the model is not just suitable for slack but also tensed systems like for tension-leg platforms. In combination with the accurate wave modelling of REEF3D, a complete toolbox for investigating complicated fluid-structure interactions is given. The influence of mooring on a floating structure was investigated for

FIGURE 10: NUMERICAL RESULTS OF THE HEAVE MOTION OVER TIME FOR THE SPHERE WITH DIFFERENT MOORING CONFIGURATIONS.

a 2D barge. It keeps the body in position and prevents intensive rolling. For the heave motion of a sphere, the influence of the mooring systems is mostly visible during the first periods. Here, shorter mooring lines increase the frequency and decrease the maximum amplitude of the motion. Both cases hint at the possible variables for an optimal design of the mooring system. Of course, the material of the ropes also plays a major role for the occurring tension forces. If the diameter increases, hydrodynamic loads on the cable should be respected as well, which is a straightforward implementation in the presented algorithm. Further research will be focused on the validation of moored-floating bodies in waves using experimental data and a systematic investigation of the influence of different mooring systems on the motion of floating bodies.

REFERENCES

[1] Davidson, J., and Ringwood, J., 2017. "Mathematical modelling of mooring systems for wave energy converters-A review". *Energies, Volume 10*, p. 666.

[2] Huang, S., 1994. "Dynamic analysis of three-dimensional marine cables". *Ocean Engineering, Volume 21*, pp. 587–605.

[3] Aamo, O., and Fossen, T., 2001. "Finite Element Modelling of Moored Vessels". *Mathematical and Computer Modelling of Dynamical Systems, Volume 7(1)*, pp. 47–75.

[4] Hall, M., and Goupee, A., 2015. "Validation of a lumped-mass mooring line model with DeepCwind semisub-

mersible model test data". *Ocean Engineering, **Volume 104***, pp. 590–603.

[5] Leitzke, H., 1983. Berechnung von Form und Kräften biegeschlaffer, räumlicher Zugsysteme. Ph.D. thesis, University of Rostock.

[6] Hackmann, W., 1983. "Mathematische Begründung von Verfahren zur Berechnung von Form und Zugkraft in Fadenzugsystemen". *ZAMM, **Volume 63***, pp. 173–184.

[7] Paschen, M., Niedzwiedz, G., and Winkel, H.-J., 2004. Fluid Structure Interactions at Towed Fishing Gears. 23rd International Conference on Offshore Mechanics and Arctic Engineering.

[8] Bihs, H., Kamath, A., Chella, M. A., Aggarwal, A., and Arntsen, Ø. A., 2016. "A new level set numerical wave tank with improved density interpolation for complex wave hydrodynamics". *Computers & Fluids, **Volume 140***, pp. 191–208.

[9] Kamath, A., Chella, M. A., Bihs, H., and Arntsen, Ø. A., 2017. "Energy transfer due to shoaling and decomposition of breaking and non-breaking waves over a submerged bar". *Engineering Applications of Computational Fluid Mechanics, **Volume 11(1)***, pp. 450–466.

[10] Kamath, A., Chella, M. A., Bihs, H., and Arntsen, Ø. A., 2015. "Evaluating wave forces on groups of three and nine cylinders using a 3D numerical wave tank". *Engineering Applications of Computational Fluid Mechanics, **Volume 9***, pp. 343–354.

[11] Grotle, E. L., Bihs, H., and Æsøy, V., 2017. "Experimental and numerical investigation of sloshing under roll excitation at shallow liquid depths". *Ocean Engineering, **Volume 138***, pp. 73–85.

[12] Berthelsen, P., and Faltinsen, O., 2008. "A local directional ghost cell approach for incompressible viscous flow problems with irregular boundaries". *Journal of Computational Physics, **Volume 227***, pp. 4354–4397.

[13] Yang, J., and Balaras, E., 2006. "An embedded-boundary formulation for large-eddy simulation of turbulent flows interacting with moving boundaries". *Journal of Computational Physics, **Volume 215***, pp. 12–40.

[14] Calderer, A., Kang, S., and Sotiropoulos, F., 2014. "Level set immersed boundary method for coupled simulation of air/water interaction with complex floating structures". *Journal of Computational Physics, **Volume 277***, pp. 201–227.

[15] Yang, J., and Stern, F., 2012. "A simple and efficient direct forcing immersed boundary framework for fluid?structure interactions". *Journal of Computational Physics, **Volume 231***, p. 5029?5061.

[16] Carrica, P., Noack, R., and Stern, F., 2007. "Ship motions using single-phase level set with dynamic overset grid". *Computers & Fluids, **Volume 36***, pp. 1415–1433.

[17] Bihs, H., and Kamath, A., 2017. "A combined level set/ghost cell immersed boundary representation for floating body simulations". *Int. J. Numer. Meth. Fluids, **Volume 83***, pp. 905–916.

[18] Kamath, A., Bihs, H., and Arntsen, Ø. A., 2017. "Study of Water Impact and Entry of a Free Falling Wedge Using Computational Fluid Dynamics Simulations". *J. Offshore Mech. Arct. Eng., **Volume 139(3)***.

[19] Sussman, M., Smereka, P., and Osher, S., 1994. "A level set approach for computing solutions to incompressible two-phase flow". *Journal of Computational Physics, **Volume 114***, pp. 146–159.

[20] Jiang, G., and Shu, C., 1996. "Efficient implementation of weighted ENO schemes". *Journal of Computational Physics, **Volume 126(1)***, pp. 202–228.

[21] Zhang, J., and Jackson, T. L., 2009. "A high-order incompressible flow solver with WENO". *Journal of Computational Physics, **Volume 228***, p. 146?159.

[22] Chorin, A., 1968. "Numerical solution of the Navier-Stokes equations". *Mathematics of Computation, **Volume 22***, pp. 745–762.

[23] van der Vorst, H., 1992. "BiCGStab: A fast and smoothly converging variant of Bi-CG for the solution of nonsymmetric linear systems". *SIAM Journal of Scientific Computing, **Volume 13***, pp. 631–644.

[24] Shu, C., and Osher, S., 1988. "Efficient implementation of essentially non-oscillatory shock-capturing schemes". *Journal of Computational Physics, **Volume 77(2)***, pp. 439–471.

[25] Osher, S., and Sethian, J., 1988. "Fronts propagating with curvature-dependent speed: Algorithms based on Hamilton-Jacobi formulations". *Journal of Computational Physics, **Volume 79***, pp. 12–49.

[26] Jiang, G., and Peng, D., 2000. "Weighted ENO schemes for Hamilton Jacobi equations". *SIAM Journal of Scientific Computing, **Volume 21***, pp. 2126–2143.

[27] Brackbill, J., Kothe, D., and Zemach, C., 1992. "A Continuum Method for Modeling Surface Tension". *Journal of Computational Physics, **Volume 100(2)***, pp. 335–354.

[28] Fossen, T., 1994. *Guidance and Control of Ocean Vehicles*. John Wiley & Sons: Chichester, England.

[29] Udaykumar, H., Mittal, R., Rampunggoon, P., and Khanna, A., 2001. "A sharp interface cartesian grid method for simulating flows with complex moving boundaries". *Journal of Computational Physics, **Volume 174***, pp. 174–345.

[30] Faltinsen, O., 1990. *Sea Loads on Ships and Offshore Structures*. Cambridge University Press, Cambridge.

[31] Ren, B., He, M., Dong, P., and Wen, H., 2015. "Nonlinear simulations of wave-induced motions of a freely floating body using WCSPH method". *Applied Ocean Research, **Volume 50***, pp. 1–12.

8